Sensors & Diagnostics

PAPER

View Article Online
View Journal

Cite this: DOI: 10.1039/d6sd00005c

Highly sensitive electrochemical sensor for uric acid using additively manufactured miniaturized microelectrodes for point-of-care applications

Sanjeet Kumar,[ac] Satish Kumar Dubey[ac] and Sanket Goel [ab]

Point-of-care (PoC) biofluid diagnostics is hindered by the fundamental limitations of traditional electrochemical platforms, namely, their complex fabrication, prohibitive costs, and reliance on benchtop instruments. To address these challenges, a simple additive manufacturing-based sensor fabrication strategy was used to develop a miniaturized platform compatible with portable electrochemical devices, creating an advanced diagnostic system capable of detecting hyperuricemia biomarkers in serum samples. In this work, a rapid and ultrasensitive diagnostic device utilizing a 3D-printed carbon conductive electrode with a carboxylic group-mediated enzymatic platform was developed to detect uric acid. This study introduces a highly sensitive 3D-printed microelectrode integrated with a wireless potentiostat for the rapid detection of uric acid (UA). The developed portable platform exhibits excellent analytical performance in the concentration range of 10–500 μM, with an ultralow detection limit of 7.95 μM achieved using chronoamperometry (CA) techniques. The device demonstrates improved selectivity, high sensitivity, and 28-day stability without interference. A real sample study was carried out using CA in a serum sample, and the recovery percentage was 97%. The results also illustrate seamless integration with a miniaturized electrochemical platform acquired using a portable potentiostat detection system and user-friendly operation. Overall, this platform enables the scalable and customizable fabrication of miniaturized biosensors, paving the way for decentralized clinical diagnostics, point-of-care testing, wearable health monitoring, and field-deployable biosensing applications.

Received 12th January 2026,
Accepted 5th May 2026

DOI: 10.1039/d6sd00005c

rsc.li/sensors

1. Introduction

Uric acid (UA) is a key clinical biomarker for the detection of gout, hyperuricemia, and chronic kidney disease. It is the final product of purine nucleotide metabolism and is primarily excreted by the kidneys.[1,2] The clinical range for UA concentration in a healthy body is typically 130 to 460 μmol (3.5–7.2 mg dL^{-1}) in males and 240 to 510 μmol L^{-1} (2.7–7.3 mg dL^{-1}) in females. These ranges can vary depending on factors such as diet, age, sex, and genetics.[3] Abnormal UA levels indicate several associated pathological conditions. Hyperuricemia, defined as UA levels exceeding 420 μmol L^{-1} in males and 360 μmol L^{-1} in females, is a significant risk factor that can lead to gout, kidney stones, hypertension, cardiovascular disease, chronic kidney disease, and metabolic syndrome.[1,2,4,5] Hypouricemia is rare, but may indicate an underlying metabolic or genetic disorder, such as Wilson's disease or Fanconi syndrome.[6] This critical clinical measure enables accurate and timely disease detection in patients, facilitating prognosis, diagnosis, management, and therapeutic monitoring.[3] Additive manufacturing, also known as three-dimensional (3D) printing, has emerged as a critical fabrication technology for the development of biosensors and other diagnostic devices.[7–11] The potential of these materials is driving research into biosensors owing to their excellent mechanical strength and necessary electrical conductivity, promising the creation of low-cost, portable platforms for point-of-care testing (POCT).[12] A few groups have successfully implemented this technology for the detection of clinical biomarkers, such as hydrogen peroxide (H_2O_2), glucose (Glu), creatinine (Cre), heavy metals, caffeine, and dopamine.[13–17] In the past few years, a few studies have been conducted using 3D-printing technology for uric

[a] MEMS, Microfluidics and Nanoelectronics (MMNE) Lab, Birla Institute of Technology and Science (BITS) Pilani, Hyderabad Campus, Hyderabad 500078, India. E-mail: sgoel@hyderabad.bits-pilani.ac.in
[b] Department of Electrical and Electronics Engineering, Birla Institute of Technology and Science (BITS) Pilani, Hyderabad Campus, Hyderabad 500078, India
[c] Department of Mechanical Engineering, Birla Institute of Technology and Science (BITS) Pilani, Hyderabad Campus, Hyderabad 500078, India.
E-mail: satishdubey@hyderabad.bits-pilani.ac.in

acid detection.[18–20] These studies have limitations, like the miniaturization of the devices, labor-intensive processes, and high operational costs. Thus, extending the 3D-printed sensing platform to integrate with portable devices is necessary for a significant research direction to offer higher sensitivity, rapid response, low cost, portability, and real-time response compared with other conventional technologies.[21–23]

Several studies have suggested that increasing the surface area of the device and utilizing various nanomaterials for sensor signal amplification can enhance electrochemical signals.[24–26] Among them, the use of gold nanoparticles,[27] graphene oxide,[28,29] and metal oxide nanomaterials, such as CuO, MnO_2, TiO_2, and Ce_3O_4,[30–32] has increased the selectivity and sensitivity of non-enzymatic biosensing applications.[16,33–35] Despite these advanced techniques, conventional UA sensors based on enzymatic and non-enzymatic methods still face difficulties, such as a low detection limit, limited portability, high sample volume requirements, poor stability, and reduced reproducibility, with restricted application for point-of-care testing.[12,17,36]

Herein, miniaturized 3D CPE electrochemical devices have been fabricated for uric acid detection. The fabricated devices were modified with DMF to increase porosity, followed by carboxylate multiwalled carbon nanotubes (MWCNTs) to enhance conductivity and electrocatalytic activity for uric acid detection. Material modification was confirmed using SEM, EDAX, and FTIR characterization techniques. An enzymatic approach was employed to detect the uricase enzyme using a specific linker. Electrochemical optimization and characterization, including electrocatalytic activity, pH effect, concentration, interference, repeatability, and reproducibility of the developed microelectrode, were carried out, and it was integrated with a portable potentiostat. Importantly, its performance was validated using a human serum sample, which achieved significant recovery values (97%) within the clinically acceptable range, thereby confirming its suitability for real sample analysis and point-of-care application in diagnostic testing.

2. Materials and methods

2.1 Materials

All chemicals used were of analytical grade. Uric acid (UA), L-ascorbic acid (AA), potassium chloride (KCl), potassium ferricyanide [$K_3Fe(CN)_6$], and uricase enzyme from *Candida* sp. (250 U) from Sigma Aldrich, India. Sodium phosphate monobasic ($NaH_2PO_4{\cdot}H_2O$), L-tryptophan (LP), sodium phosphate dibasic ($Na_2HPO_4{\cdot}H_2O$), glucose, sodium chloride (NaCl), and creatinine (Cr), each with a purity of approximately 99.9%, were used and purchased from Sigma Aldrich, India. Multiwalled carbon nanotubes (MWCNTs) were procured from TCI India. Dimethylformamide (DMF) [$HCON(CH_3)_2$] was used as the organic solvent for the electrode-surface activation. EDC (1-ethyl-3-(3-dimethylaminopropyl)carbodiimide) and NHS (*N*-hydroxysuccinimide) were obtained from Sigma-Aldrich, India. All solutions were prepared using deionized water with a resistivity of 18.2 MΩ cm.

2.2 Instruments

Various instruments have been utilized for device fabrication and electrode characterization. Electrochemical device characterization was carried out using a model SP-150 potentiostat and a portable Sensit BT potentiostat purchased from BioLogic Science Instruments (France) and Sensit BT, Palmsens (Netherlands), respectively. A dual-extruder 3D printer, the BCN3D Sigma D25 model, manufactured by BCN3D, Lleida, Spain, was used for the fabrication process. The printer features an Independent Dual Extruder (IDEX) architecture, enabling multi-material and multi-color printing with a build volume of 420 mm × 300 mm × 200 mm. Scanning electron microscopy (SEM) was used for surface morphology studies using an Apreo SEM instrument procured from Thermo Fisher Scientific (USA). Electrically conductive composite polylactic acid (PLA) filaments (2.85 mm, black) were purchased from Protopasta 3D Filaments (Vancouver, USA). The pH measurement was carried out using a double junction pH meter procured from the Oakton 700 pH electrode (Singapore). A silver–silver chloride (Ag/AgCl) paste was procured from ALS, Japan. Non-conducting polylactic filament (PLA) was purchased from BCN3D Filaments (Lleida, Spain).

2.3 Design and fabrication of 3D printed conductive electrodes

The electrode geometry was designed in SolidWorks (Student Version 2024) and exported in stereolithography (.stl) format, followed by a slicing software to print the geometry (G code), as shown in Fig. 1(a and b). The device was printed using a fused deposition modeling (FDM)-based 3D printing approach using a dual extrusion 3D printer with 0.4 mm nozzles operating at 210 °C. A non-conductive PLA filament was used to form the base structure. In contrast, a carbon-loaded conductive PLA filament was used to print the integrated three-electrode system, comprising a working electrode (WE), a reference electrode (RE), and a counter electrode (CE), as shown in Fig. 2(a–c). The final printed electrode had a rectangular footprint of 25 mm × 11 mm, with a thickness of 0.5 mm. A 5 mm × 5 mm sample reservoir was incorporated into the design to confine the analyte solutions. After fabrication, the printed electrodes were treated with dimethylformamide (DMF) for 5 minutes to enhance their surface wettability and electrocatalytic activity, followed by rinsing with deionized (DI) water and air drying. DMF treatment induces swelling and partial dissolution of the PLA matrix, leading to the exposure of embedded conductive fillers and the formation of micro-/nano-porous structures upon solvent evaporation, thereby enhancing

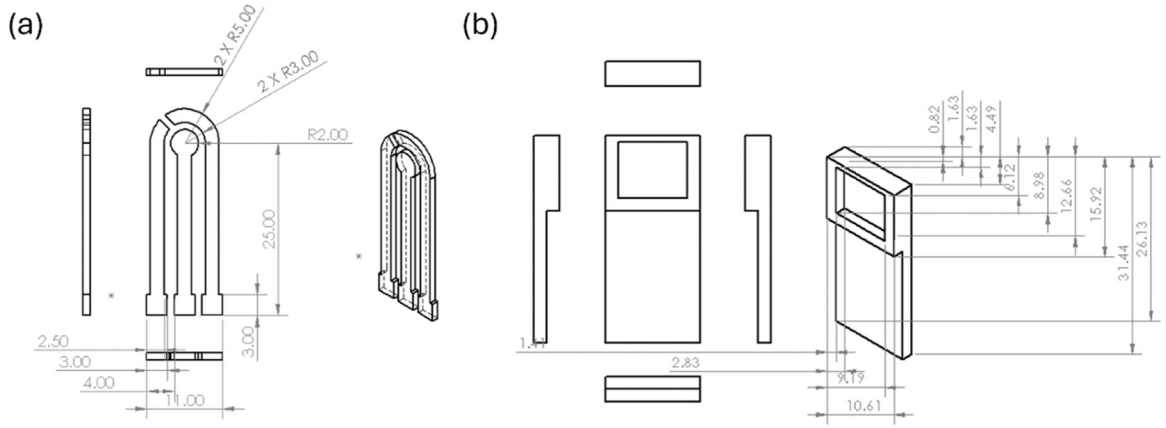

Fig. 1 (a) Schematic illustration of the dimensions of the developed three-electrode system. (b) Front, side, and back views of the fabricated microelectrode with the corresponding dimensional specifications.

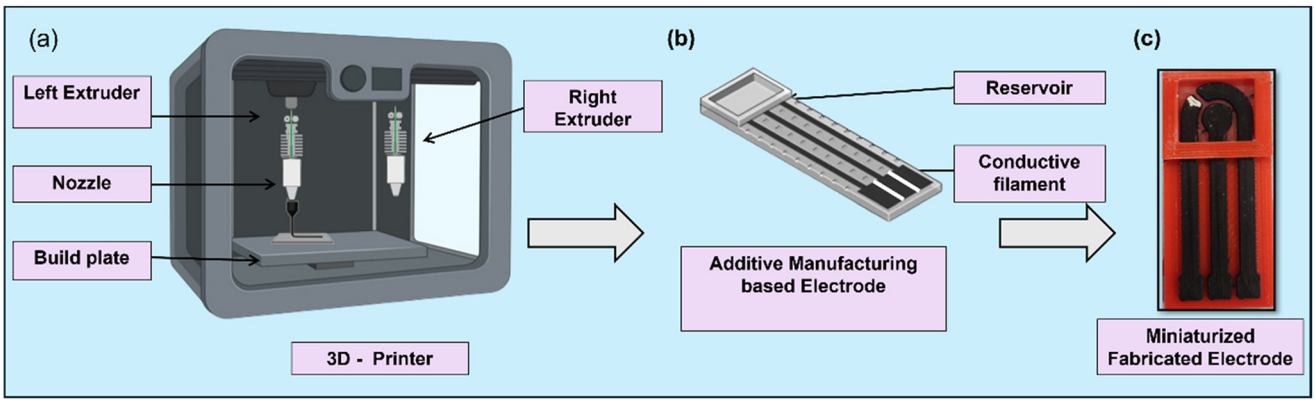

Fig. 2 (a) Fabrication of an electrochemical sensor using carbon conductive electrodes with 3D-printing (BCN 3D printer). (b) Printed electrode with the sample reservoir and conductive electrodes using additive manufacturing. (c) Final fabricated miniaturized electrodes.

the effective electroactive surface area. Similar morphological changes induced by solvent treatment were observed in the polymer composites. Each print cycle produced 20 identical sensor devices in a single run using the dual-extrusion 3D printer. All the 20 electrodes from a given print were subjected to the same surface modification and functionalization protocol in batches (identical reagent volumes, incubation times, and washing steps). To minimize electrode-to-electrode variability, all the printing parameters were kept constant across batches: printing speed (50% of the printer's rated speed), nozzle temperature (220 °C), layer height, infill density, and extrusion flow rate.

2.4 Analyte and enzyme preparation

All solutions were prepared in a freshly prepared 0.1 M phosphate buffer solution (pH 7.0) to support the entire electrolyte for the voltammetric and chronoamperometric detection of uric acid. A stock solution of uric acid was prepared in 0.1 M PBS, and various concentrations were obtained by diluting the stock solution. The uricase enzyme was also prepared in 0.1 M PBS (pH 7), where the uricase was taken as 1 mg in 1 mL of PBS, a freshly prepared solution during the experimental procedure. Additionally, a multiwalled carbon nanotube was prepared using 10 mg of MWCNT powder in 1 mL of ethanol (99% pure). A 30 : 10 ratio of EDC and NHS was also used for electrode modification to activate the electrode surface with carboxyl groups, which could then be used for the covalent binding of the uricase enzymes.

2.5 Sensing mechanism

The electrochemical sensing mechanism for uric acid was facilitated through a biocatalytic mechanism using uricase enzymes immobilized onto a 3D-CPE printed electrode surface. The working electrode was modified with multiwalled carbon nanotubes (MWCNTs) to increase the electroactive surface area of the electrode and electron transfer. EDC and NHS were employed on the electrode surface area to enhance the immobilization of the uricase enzyme and facilitate its proper binding. The uricase enzyme catalyzes the oxidation of uric acid to allantoin with the production of hydrogen peroxide (H_2O_2) and the generation of H_2O_2 and carbon dioxide (CO_2); the reaction mechanism is shown in eqn (1).

$$\text{Uric Acid} + O_2 + H_2O \xrightarrow{\text{Uricase}} \text{Allantoin} + CO_2 + H_2O_2 \quad (1)$$

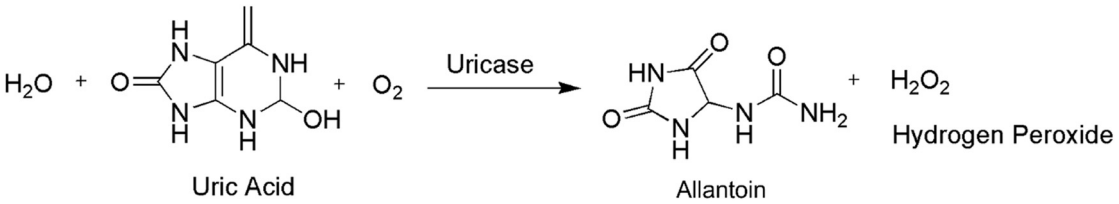

The generated H_2O_2 is electrochemically active and undergoes further oxidation at the electrode surface, producing a measurable current response that is proportional to the uric acid concentration.

2.6 Electrode modification

Electrode modification was carried out using dropcasting techniques. Initially, the electrode was treated with a 0.1 M solution of dimethylformamide (DMF) to increase the porosity of the working electrodes. Later, a 10 mg mL^{-1} solution of carboxylated multiwalled carbon nanotubes (MWCNTs) was prepared in pure ethanol (99.99%) and kept in a water bath to facilitate the dispersion of the solution. Afterward, the crosslinker was prepared in a 30 : 10 ratio of 0.2 M EDC and 0.05 M NHS and dissolved in 0.1 M PBS (pH 7). A volume of 20 μL was dropcast after MWCNT modification. Finally, the uricase enzyme was prepared in a 1 mg mL^{-1} solution of PBS (pH 7). A 10 μL volume of the prepared solution was dropcast on the working electrode area and kept at 4 °C overnight, as depicted in Fig. 3. Subsequently, all the electrochemical detections were carried out.

3. Results and discussion

To test the performance of the sensor and the structural features of the developed miniaturized devices, including their structural properties and electrochemical performance of the 3D-CPE biosensor, the morphological characterization of the sensor was carried out using SEM, EDX, and FTIR to confirm the electrode functionalization. Electrochemical characterization was carried out using cyclic voltammetry (CV) and chronoamperometry (CA) techniques.

3.1 Material characterization

To understand the electrode characterization upon each successful stepwise modification for the 3D-CPE devices, scanning electron microscopy (SEM), energy dispersive X-ray spectroscopy (EDX), and modification of the functional group at each stage were carried out using Fourier transform infrared spectroscopy (FTIR). All the elaborative studies are presented in the following subsections.

3.1.1 FE-SEM analysis. Morphological studies of the electrode surface area were conducted using field-emission scanning electron microscopy (SEM). Initially, the samples were kept for gold coating using gold coater instruments for each of the samples prepared, up to 15 nm. As shown in Fig. 4(a), bare 3D-CPE was conducted, which exhibits a relatively limited microstructural feature. As shown in Fig. 4(b), DMF-treated electrodes show a rougher and more porous surface morphology, characterized by increased surface texture and microvoids. Fig. 4(c) and (d) show modification with multiwalled carbon nanotubes, which are evenly distributed on the electrode surface, with magnifications of 10 μm and 500 nm, respectively.[37] These results show an increase in surface area and a change in

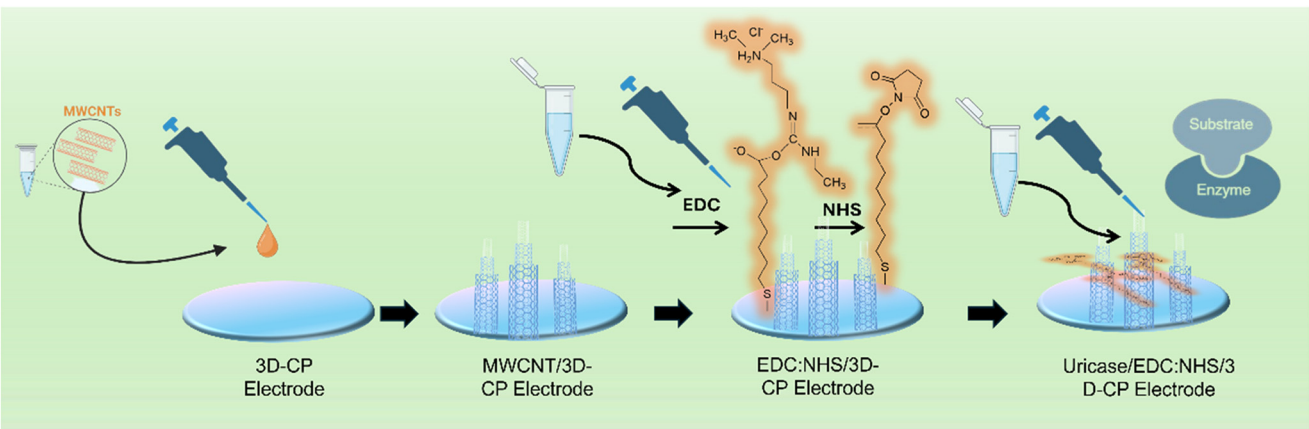

Fig. 3 Schematic of the stepwise electrode surface modification for uric acid (UA) detection.

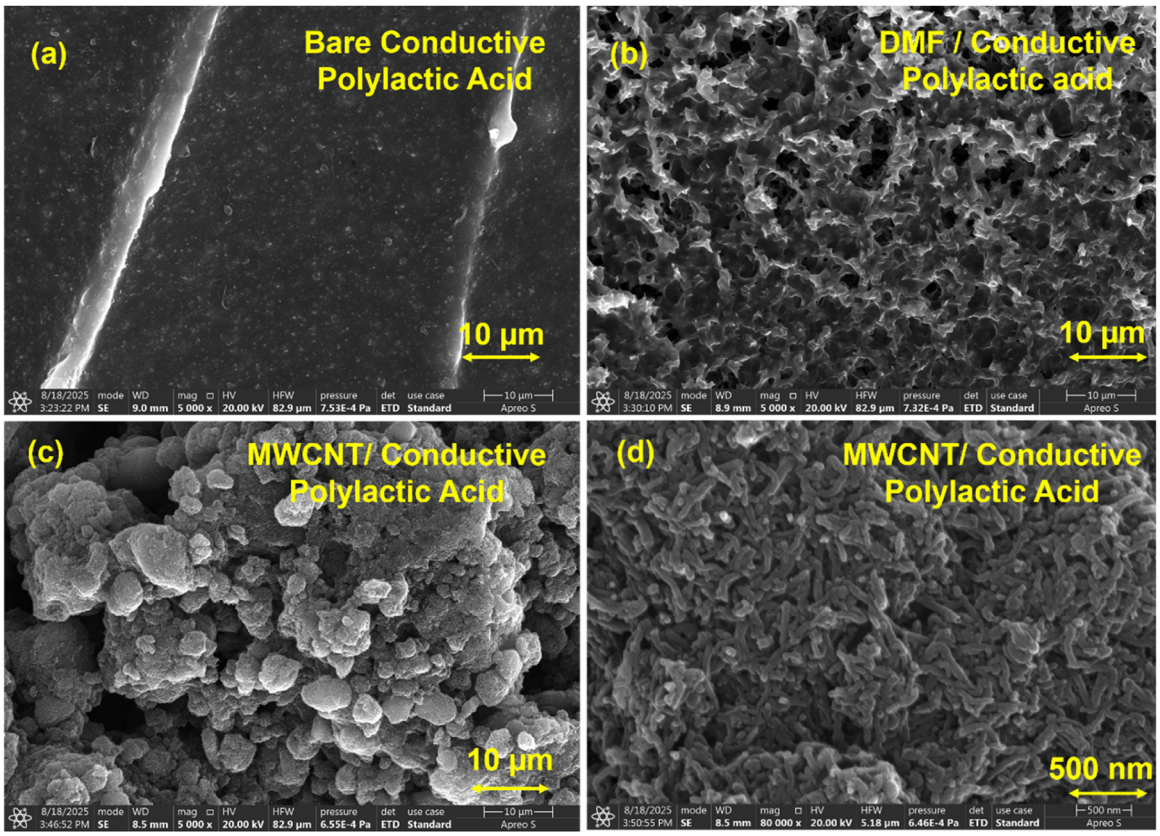

Fig. 4 FE-SEM images of the working electrodes: (a) bare 3D-CPE under a magnification of 10 μm, (b) DMF-treated 3D-CPE under a magnification of 10 μm, showing the increased surface porous nature, and (c) and (d) MWCNT-modified 3D-CPE, under magnifications of 10 μm and 500 nm, respectively.

porous nature with modification, which benefits electrochemical sensor applications.

3.1.2 EDX analysis. The elemental composition of the modified material was confirmed using energy dispersive X-ray spectroscopy (EDX), which was employed to analyze the 3D-CPE device at each stage of surface modification. As shown in Fig. 5(a) and (d), the bare 3D-CPE, with an elemental composition of carbon (C) and oxygen (O), presents atomic percentages of 80.65% and 19.35%, respectively, with a carbonaceous base structure. As depicted in Fig. 5(b) and (e), the electrode surface was modified with DMF, and the elements present were C, O, Si, and S, which are additional elements, with atomic percentages of 80.27%, 18.95%, 0.38%, and 0.40%, respectively. As illustrated in Fig. 5(c) and (f), the modification of the MWCNTs shows an increase in the atomic percentage of carbon elements to 91.68% and a decrease in the oxygen elements to 8.32%, indicating that the increased percentage of elements leads to better electrochemical studies.

3.1.3 XPS analysis. X-ray photoelectron spectroscopy (XPS) analysis was performed to confirm the elemental composition and chemical states of the 3D-CPE. The XPS survey for the 3D-CPE confirms the presence of elements C and O, as shown in Fig. 6(a). The presence of the C 1s spectrum, as shown in Fig. 6(b), confirms a peak at 284.8 eV for C–C. Subsequently, fitting was carried out using Avantage software (Thermo Fisher Scientific) to verify the deconvolution of the carbon elements at the peak for C–O–C at 286 eV. The O–C═O peak at 288.5 eV indicates a graphitic structure, and the functional group helps enhance electron transfer and provide proper immobilization. The O 1s XPS spectrum of the modified electrode (Fig. 6(c)) was deconvoluted into two main components centered at ~531.8 eV and ~533.3 eV. The peak at ~531.8 eV is assigned to C═O groups, including carbonyl and amide functionalities, which indicates the formation of covalent linkages between the carboxyl groups of MWCNT and amine groups of uricase *via* EDC/NHS coupling. The second component at ~533.3 eV corresponds to C–O/O–C–O species, arising from hydroxyl or epoxy groups present on the carbon surface. A minor high binding energy tail (~534 eV) is also observed, which is attributed to adsorbed water or oxygen species.[38] These bonds, as presented in the XPS survey, help improve hydrophilicity and charge transfer, thereby enhancing electrochemical sensing.

3.1.4 Fourier transform infrared spectroscopy (FTIR) analysis. Fourier transform infrared spectroscopy was employed to confirm the sequential surface modifications of the 3D electrode during fabrication. The FTIR spectrum of the DMF-treated electrode exhibited characteristic peaks

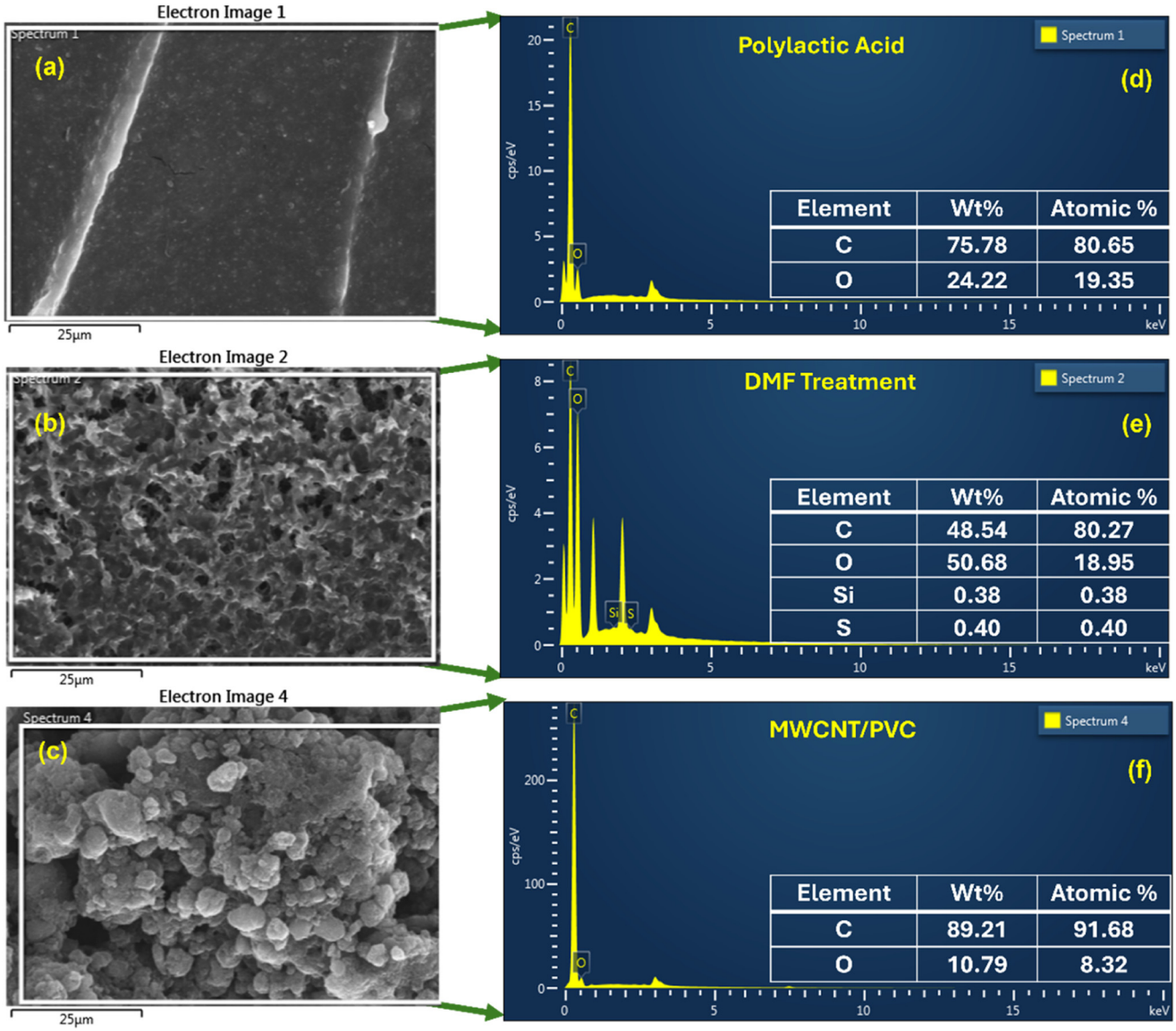

Fig. 5 EDX analysis of (a and d) bare 3D-CPE (inset: elemental composition of C and O), (b and e) DMF-treated 3D-CPE (inset: elemental composition of C, O, Si, and S), and (c and f) MWCNT-coated 3D-CPE (inset: elemental composition of C and O).

around 1640 cm^{-1} and 1400 cm^{-1}, corresponding to C═O stretching (amide) and C–N bending vibrations, respectively, which indicates partial surface activation and interaction of DMF with the electrode matrix, as shown in Fig. 7. Upon modification with multiwalled carbon nanotubes (MWCNTs), a prominent peak at approximately 1570 cm^{-1} was observed, attributed to C═C stretching vibrations from the graphitic backbone of MWCNTs, along with a broad O–H stretching band around 3400 cm^{-1}, indicating the presence of hydroxyl groups from surface oxidation. Subsequent activation using EDC/NHS chemistry introduced new peaks near 1740 cm^{-1} and 1380 cm^{-1}, which were assigned to ester C═O stretching and N–O symmetric stretching, respectively. These peaks are characteristics of the successful formation of NHS esters and confirm the activation of carboxyl groups for amide bond formation. Finally, after uricase immobilization, two new bands emerged at ~1655 cm^{-1} and ~1540 cm^{-1}, corresponding to the amide I (C═O stretching of the peptide bond) and amide II (N–H bending and C–N stretching) vibrations, respectively, which indicate protein secondary structure and confirm the successful covalent attachment of the enzyme on the electrode surface.

3.2 Analytical performance of a 3D-CPE printed electrode towards uric acid

3.2.1 Electrochemical behaviour of the device using a redox mediator. Cyclic voltammetry (CV) was performed using a standard 5 mM $[Fe(CN)_6]^{3-/4-}$ redox probe in 0.1 M KCl to evaluate the electrochemical activity and electron transfer kinetics of the 3D-CPE electrode at various stages of

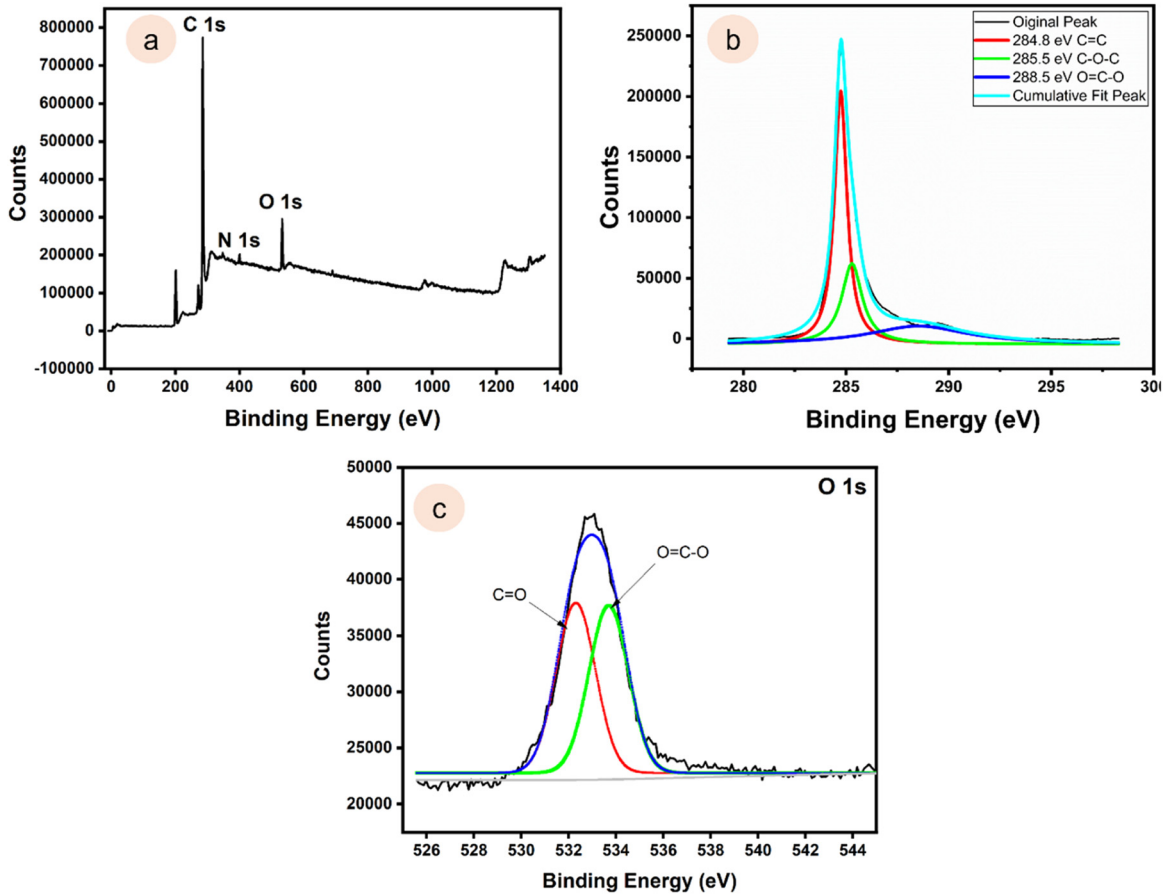

Fig. 6 XPS analysis of the 3D-printed carbon-conductive polylactic electrode (3D-CPE): (a) full survey spectrum showing the presence of the C 1s and O 1s peaks, (b) high resolution C 1s spectrum deconvoluted into C–O–C and O–C═O at 284.8 eV, and (c) O 1s high-resolution XPS spectrum showing the deconvoluted peaks at ~531.8 eV and ~533.3 eV, corresponding to the C═O and C–O/O–C–O functional groups, respectively.

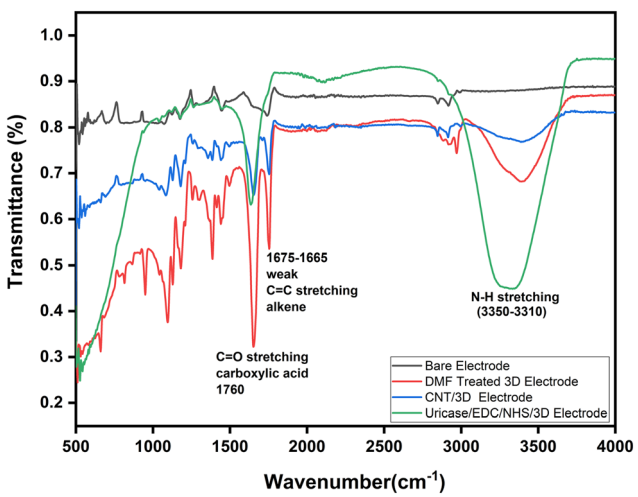

Fig. 7 FTIR spectra of the 3D electrodes at different stages of surface modification: bare electrode, DMF-treated electrode, MWCNT-modified electrode, EDC/NHS-activated surface, and uricase-immobilized electrode. Characteristic peaks corresponding to the functional groups confirm the successful stepwise modification and enzyme immobilization.

modification. The bare electrode exhibited well-defined redox peaks with moderate peak-to-peak separation (ΔE_p), indicating quasi-reversible behaviour. Upon modification with MWCNTs, a significant increase in peak current and a decrease in ΔE_p were observed, suggesting enhanced electron transfer due to the nanotube's high conductivity and increased surface area. Further, functionalization with EDC/NHS and uricase resulted in a slight decrease in peak current attributed to partial electrode surface blocking by the biomolecular layer, as shown in Fig. 8(a). These results confirm the successful modification of the electrode and the preservation of the electrochemical activity necessary for biosensing applications.

3.2.2 Optimization of pH effect study for uric acid. The effect of pH on the electrochemical response of uric acid was investigated using cyclic voltammetry (CV) in 0.1 M phosphate buffer (pH 3–10) containing 500 μM of uric acid. The CV study shows a strong pH dependence due to the proton occurring in the redox mechanism. At pH (3–5), redox peaks, with low current observed, are attributed to the protonation of uric acid and hinder electron transfer. Increasing the pH from 6 to 9 resulted

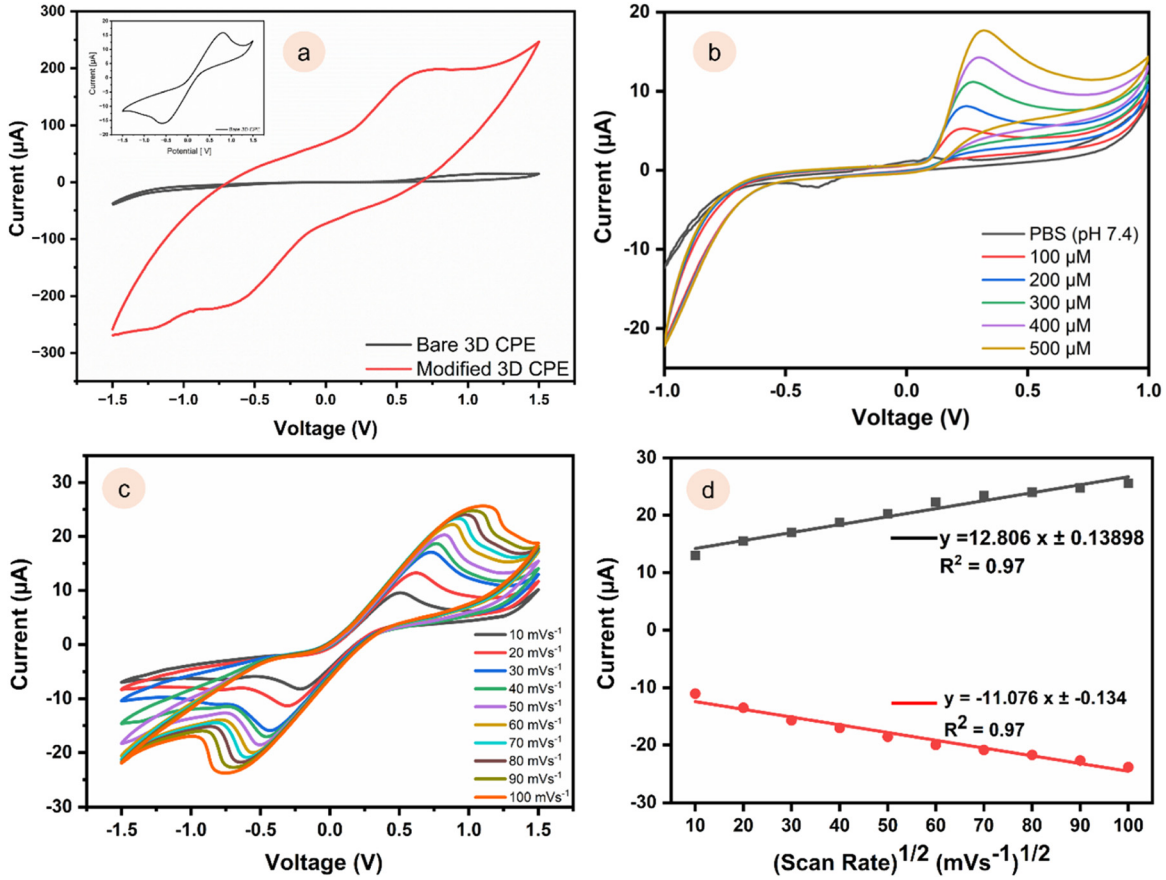

Fig. 8 (a) CV responses of a 3D-CPE electrode for device performance using 5 mM $K_3[Fe(CN)_6]$ in a 1 M KCl solution. Inset: CV response of the bare 3D-CPE electrode in the range of −1.5 to 1.5 V at 50 mV s^{-1}. (b) CV responses of electrodes in the presence of PBS (pH 7) and (1000 μM) uric acid at 50 mV s^{-1} on the electrode surface of uricase/MWCNT/3D-printed carbon conductive filament-based electrode (3D-CPE). (c) CV responses of various scan rates of uric acid detection from 10 mV s^{-1} to 100 mV s^{-1}. (d) Corresponding calibration curve plots for the I_{pa} *vs.* $(\text{scan rate})^{1/2}$ $(\text{mV s}^{-1})^{1/2}$.

in enhanced anodic currents and a negative shift in oxidation potential, consistent with the proton-coupled electron transfer (PCET) process. At pH 7, well-defined redox peaks with a maximum current response were obtained, indicating optimal electron transfer kinetics and molecular stability. Beyond pH 9, peak broadening suggested uric acid instability in alkaline media. Therefore, pH 7 was selected under optimal working conditions, providing both physiological relevance and stable electrochemical performance.

3.2.3 Cyclic voltammetry responses to uric acid. The electrochemical behaviour of the device was tested with 1 mM of 50 μL uric acid solution by the CV in 0.1 M phosphate buffer solution (PBS) of pH 7 in the optimized potential window of 1 V to −1 V at a scan rate of 50 mV s^{-1}, and the sample volume is 50 μL. The CV response was recorded for the bare 3D-CPE and uricase/EDC/NHS/MWCNT/modified 3D printed carbon conductive filament-based electrode (3D-CPE) with PBS in the presence of uric acid at a scan rate of 50 mV s^{-1}, as depicted in Fig. 8(b). In the response for the bare 3D CPE for the uric acid, there was no significant peak observed, while for the modified Uricase/EDC: NHS/MWCNT/modified 3D CPE electrode, a significant oxidation peak was observed at 0.31 V, as reported in the works, indicating that uric acid undergoes oxidation with the developed device.[20,27,31,39]

3.2.4 Effect of scan rate study. Cyclic voltammetry was performed at varying scan rates ranging from 10 to 100 mV s^{-1} in the presence of 0.5 mM K_3 $[Fe(CN)_6]^{3-/4-}$ in 1 M KCl within the potential window of −1.5 to +1.5 V, as shown in Fig. 8(c). The ferri/ferrocyanide redox couple exhibited well-defined anodic and cathodic peaks, both of which increased proportionally with the square root of the scan rate, confirming diffusion-controlled electron transfer. The corresponding calibration plots of the anodic and cathodic peak currents *versus* the square root of the scan rate displayed linear relationships, as shown in Fig. 8(d). This behaviour is consistent with the Randles–Ševčík equation for reversible systems:

$$I_{pa} = 2.69 \times 10^5 n^{3/2} A D^{1/2} C v^{1/2}, \quad (2)$$

where $I_{pa}/v^{1/2}$ is the slope calculated from the calibration graph 12.806 μA/$(\text{mV s}^{-1})^{1/2}$, n is the number of electrons participating in the reaction (assumed to be 1). The

geometric area of the working electrode (WE), based on a 4 mm diameter, was calculated to be 0.126 cm^2. Using the scan rate, the diffusion coefficient (D) was determined using the Randles–Ševčík equation, and the calculated diffusion coefficient was found to be (D) (cm^2 s^{-1}) 5.74×10^{-7} cm^2 s^{-1}, the analyte concentration (C) (mol cm^{-3}) was 0.5 mM, and the scan rate (mV s^{-1}), which is in reasonable agreement with reported values for the ferri/ferrocyanide system, confirming the reliability of the electrochemical response. The strong linearity indicates that the fabricated electrode provides efficient and stable electron transfer characteristics.

3.2.5 Effect of concentration study. To evaluate the sensitivity and analytical performance of the developed sensor, the uric acid concentration-dependent electrochemical response was studied using the chronoamperometric (CA) technique. The measurements were conducted under optimized conditions at an anodic potential of 0.31 V (determined from cyclic voltammetry) for 60 s, with a sample volume of 50 μL. The concentration study was carried out in the range of 10–500 μM, as shown in Fig. 9(a). A gradual increase in the current response was observed with increasing uric acid concentration, confirming the efficient catalytic oxidation of uric acid by the uricase-modified 3D printed carbon conductive filament-based electrode (3D-CPE). This reaction indicates the proper electrocatalytic activity of uric acid to allantoin, carbon dioxide, and hydrogen peroxide (H_2O_2), where uricase, as the enzyme used, is described by the following enzymatic reaction mechanism.

$$\text{Uric acid} + O_2 + H_2O \xrightarrow{\text{Uricase}} \text{Allantoin} + CO_2 + H_2O_2$$

The generated hydrogen peroxide (H_2O_2) undergoes electrochemical oxidation at the electrode surface, producing an anodic current proportional to the uric acid concentration.

$$H_2O_2 \rightarrow 2H^+ + O_2 + 2e^-$$

This redox process behaviour of the device mechanism, where the current increases, demonstrates the oxidation of enzymatically produced H_2O_2. The calibration plot with the correlation coefficients of R^2 = 0.99, indicating proper linearity, as shown in Fig. 9(b). Based on the slope and standard deviation (σ) of the calibration curve, the limit of detection (LOD) and limit of quantification (LOQ) were calculated using the following equations:[40,41]

$$\text{LOD} = 3.3 \times \frac{\sigma}{S}, \quad (3)$$

$$\text{LOQ} = 10 \times \frac{\sigma}{S}. \quad (4)$$

The calculated LOD and LOQ values were 7.95 μM and 24.11 μM, respectively, demonstrating the capability of the sensor for trace level detection of uric acid.

3.2.6 Interference study. The selectivity of the uricase-modified 3D-CPE sensor was investigated for 100 μM uric acid in the presence of physiologically relevant interferents, including creatinine (50 μM), ascorbic acid (10 μM), urea (100 μM), lactate (1 mM), glucose (5 mM), K^+ (4 mM), and Na^+ (130 mM). Chronoamperometric (CA) measurements were performed in 0.1 M phosphate-buffered saline (PBS, pH 7) at an applied potential of +0.31 V for 60 s using a sample volume of 100 μL. As shown in Fig. 10(a), the current response for uric acid exhibited negligible variation after the sequential addition of these potential interferents, with a relative standard deviation (RSD) of 3.5%. These results demonstrate that the developed biosensor possesses excellent selectivity toward uric acid detection, even in the presence of coexisting electroactive or ionic species.

3.2.7 Repeatability, reproducibility, and stability of the device. The repeatability of the uricase-modified 3D-CPE sensor was evaluated using chronoamperometric (CA) measurements under optimized conditions. Ten successive

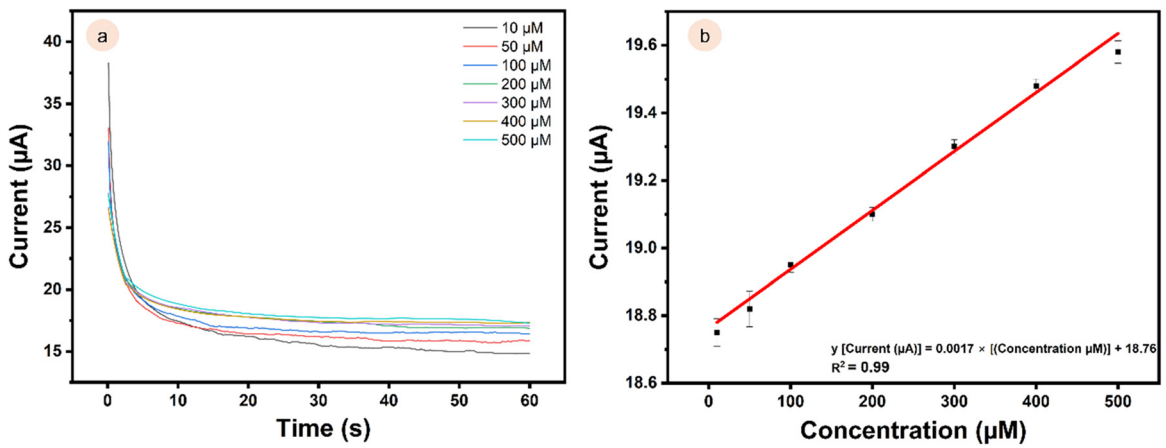

Fig. 9 (a) Chronoamperometric responses of the uricase-modified 3D (3D-CPE) recorded at different uric acid concentrations (10–500 μM) under an applied potential of 0.31 V for 60 s. (b) Corresponding calibration plot showing a linear relationship between the current response and uric acid concentration (R^2 = 0.99).

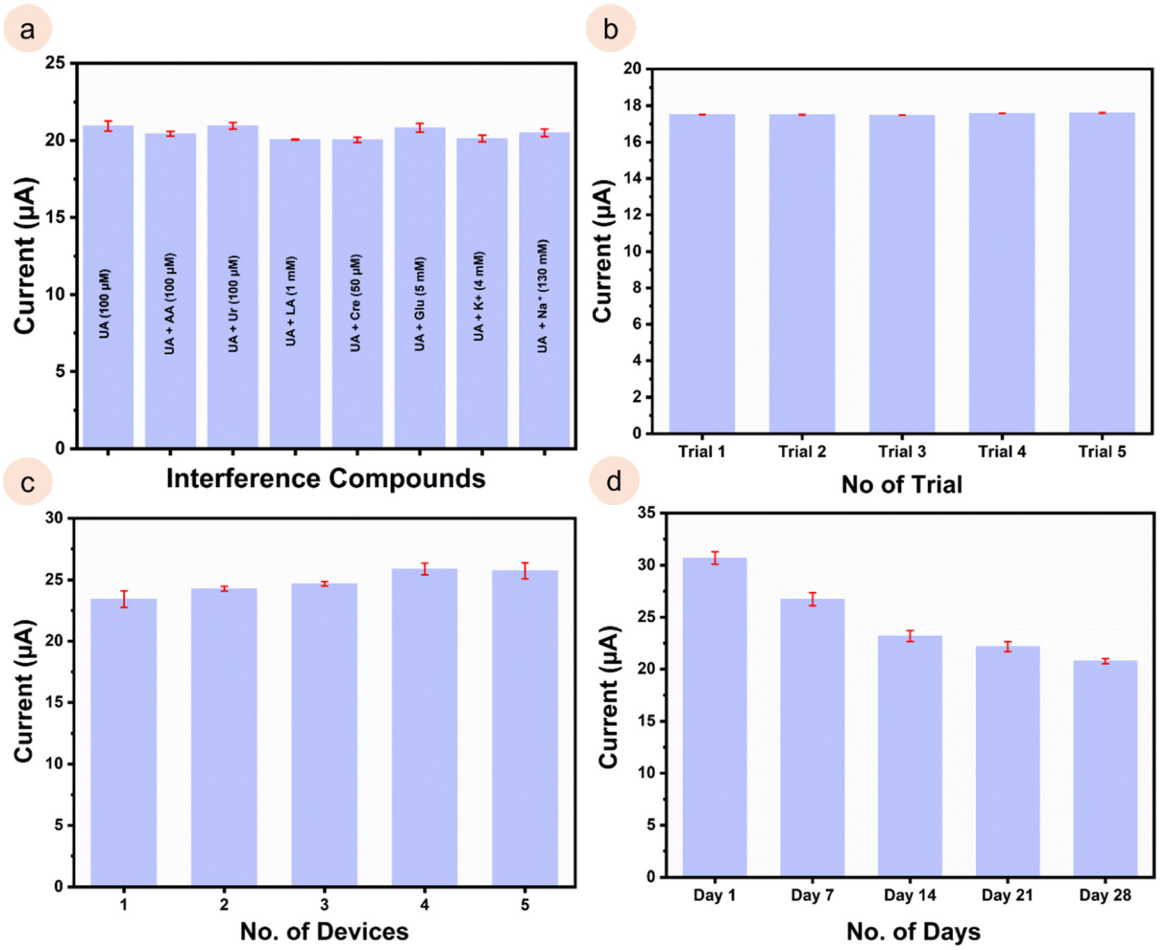

Fig. 10 (a) Chronoamperometric (CA) responses of the uricase-modified 3D-CPE sensor toward 100 μM uric acid in the presence of potential interferents, including creatinine, ascorbic acid, urea, lactate, glucose, K^+, and Na^+ ions, recorded in 0.1 M PBS (pH 7) at +0.31 V for 60 s. (b) Repeatability study carried out using the chronoamperometric responses of a single uricase-modified 3D-CPE for ten successive additions of 300 μM uric acid in 0.1 M PBS (pH 7) at +0.31 V, showing highly consistent currents (RSD = 3.8%) (n = 3). (c) Reproducibility study carried out using five independently prepared uricase-modified 3D-CPEs for 300 μM uric acid under identical conditions, demonstrating minor variations in current (RSD = 4.2%) (n = 3). (d) Storage stability study carried out using the chronoamperometric response of the biosensor to 300 μM uric acid over 28 days with the electrodes stored at 4 °C in 0.1 M PBS, retaining ~92% of the initial current after two weeks. The experiments were carried out in triplets.

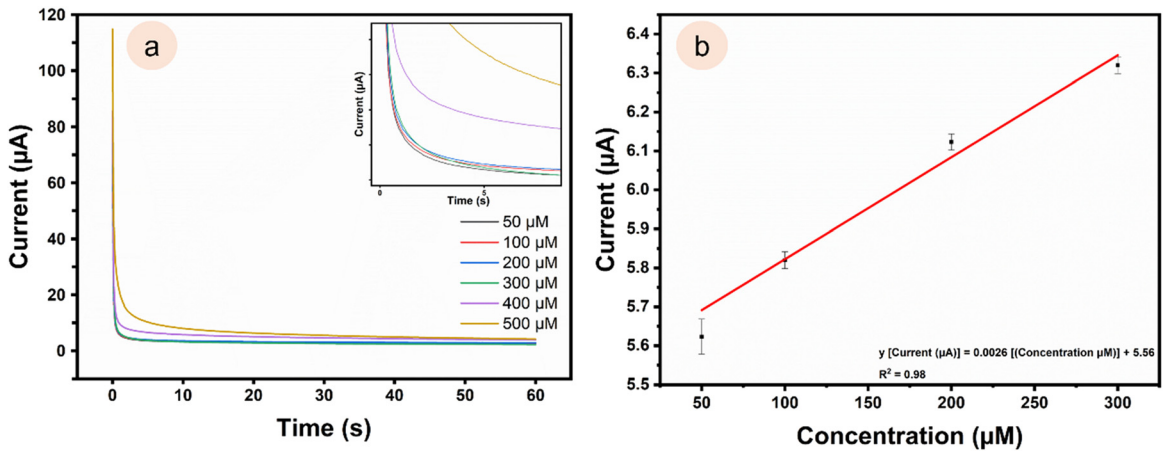

Fig. 11 (a) Concentration study using a portable potentiostat in the range of 50 to 500 μM, inset: enlarged view. (b) Corresponding calibration plot (R^2 = 0.98). The experiments were carried out in triplets (n = 3).

chronoamperometric responses were recorded for 300 μM uric acid in 0.1 M PBS (pH 7) at an applied potential of +0.31 V for 60 s. The current responses remained highly consistent, exhibiting a relative standard deviation (RSD) of 3.8%, confirming excellent signal repeatability, as shown in Fig. 10(b). The negligible variation in current across repeated measurements indicates minimal electrode fouling and stable electron transfer kinetics at the modified electrode surface. To evaluate fabrication reproducibility, five independent uricase-modified 3D CPE electrodes were prepared using the same protocol. Their CA responses toward 300 μM uric acid were recorded under identical conditions. The oxidation peak currents showed only minor variations, with a relative standard deviation (RSD) of 4.2%, as shown in Fig. 10(c). This low RSD demonstrates reliable electrode preparation and consistent enzyme immobilization, which is essential for large-scale sensor fabrication. The storage stability of the biosensor was evaluated by monitoring its chronoamperometric response to 300 μM uric acid at regular intervals over 28 days. When not in use, the electrodes were stored at 4 °C in 0.1 M phosphate buffer (pH 7). The steady state current decreased gradually, retaining approximately 92% of the initial response after two weeks. This minimal loss indicates that both the enzymatic activity of the uricase and the structural integrity of the modified electrode were well preserved under storage conditions. The observed stability is comparable to or better than previously reported enzymatic biosensors, which typically exhibit a 10–15% decrease in activity over a similar period, as shown in Fig. 10(d).

3.2.8 Portable device validation. The concentration study was also carried out using a portable potentiostat (detail in the equipment section), as shown in Fig. 11(a and b). Chronoamperometry techniques were carried out at an anodic potential of 0.31 V for 60 s, with a concentration range of 50–500 μM and a sample volume of 50 μL. The calculated linear response was observed in the range of 50–500 μM, and a coefficient of correlation of 0.98 was obtained, confirming linearity. The limits of detection and quantification were also calculated to be 7.4 μM and 22.4 μM, respectively. The portable Sensit BT potentiostat exhibits a higher LOD compared to the benchtop system, primarily due to its higher noise floor, lower current resolution, and limited amplifier sensitivity, which reduce the signal-to-noise ratio at low analyte concentrations. Despite this, the device demonstrates good linearity within the 50–300 μM range, which is relevant for practical point-of-care applications.

3.2.9 Real sample analysis. The practical applicability of the uricase-modified 3D-CPE was demonstrated through chronoamperometric analysis of spiked human serum samples. Samples were diluted appropriately in 0.1 M PBS (pH 7), and CA measurements were carried out at an applied potential of +0.31 V. The known concentrations of uric acid were added to the samples, and the corresponding current responses were recorded, as shown in Fig. 12(a and b). The biosensor exhibited rapid, well-defined, and concentration-dependent currents, enabling accurate quantification. Recovery studies yielded values of 97% for serum samples, indicating excellent accuracy, as shown in Table 1. These results confirm that the enzymatic activity of the uricase and the structural integrity of the modified electrode are maintained in complex biological matrices, highlighting the potential of the developed device for reliable clinical and diagnostic applications. A summary of previous studies on enzymatic electrochemical detection of uric acid is presented in Table 2.

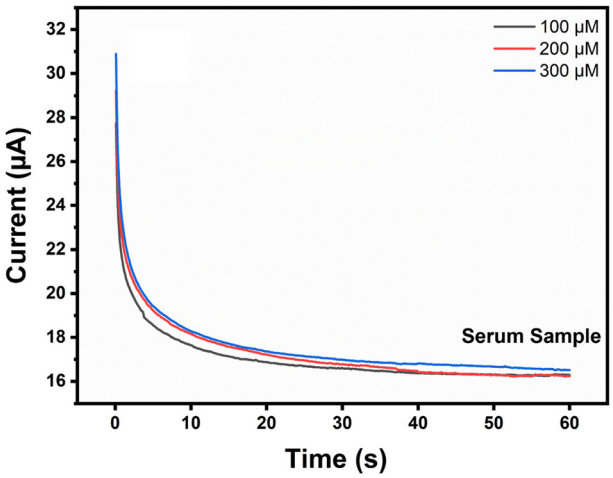

Fig. 12 Chronoamperometric analysis of the uricase-modified 3D-CPE in real samples: (a) human serum spiked with known concentrations of uric acid. The sensor exhibits rapid, concentration-dependent current responses with recoveries of 97% for serum, demonstrating excellent accuracy and applicability in complex biological matrices.

Table 1 Real sample analysis

#	Sample	Added (μM)	Found (μM)	Recovery
1	Serum	100	97.06	97.06%
		200	193.53	96.77%
		300	290.59	96.86%

Recovery percentage (%) = (Added/Found) × 100.[42–44]

4. Conclusion

This work presents a miniaturized and portable electrochemical device fabricated through a simple one-step 3D printing approach for uric acid detection. A highly sensitive sensing platform was achieved by directly integrating working, counter, and reference electrodes from commercial conductive polylactic acid filaments and further functionalizing them with multi-walled carbon nanotubes (MWCNTs), EDC/NHS coupling, and uricase. A well-defined oxidation potential at ~0.31 V was observed, and the device was systematically optimized with respect to pH, concentration, scan rate, interference, and stability. A wide

Table 2 Analytical performance of the present sensor compared with reported uric acid sensors

#	Fabrication technique	Sensor modification	Linear range (μM)	LOD (μM)	Portability/instrumentation	Ref.
1.	Glassy carbon electrode	Nanotube paste electrode (enzymatic)	20–380	0.18	Benchtop system	45
2.	Glassy carbon electrode	CuO/GCE non-enzymatic sensor	1–400	0.6	Bulky system	46
3.	3D-printed	3D SACNT	100–1000	10	Benchtop	47
4.	Screen-printed electrode	AC/VCO/BW/SPE	10–1000	43.8	Bulky system	47
5.	Screen-printed electrode	MC-ZnO/SPE	20–225	3.76	Bulky system	48
6.	Glassy carbon electrode	Fe_3O_4/GCE	20–160	14	Bulky system	40
7.	Carbon paste electrode	ZnO/PANI/CPE	10–120	7	Bulky system	14
8.	ECL	MoS_2 QDs	100–500	20	Benchtop system	49
9.	ITO	Uricase/CNT/Pani	100–1000	43.2	Benchtop system	50
10.	Glassy carbon electrode	AuNPs@MoS_2	50–40 000	10	Bulky system	27
11.	Carbon conductive 3D-CPE	MWCNT/EDC/NHS/uricase-modified 3D-CPE	10–500	7.95 μM	Miniaturized PoC devices (Sensit-BT Potentiostat)	**This work**

Abbreviations: AuNPs: gold nanoparticles, ITO: indium tin oxide, ECL: electrochemiluminescence, ZnO: zinc oxide, MoS_2: molybdenum disulfide, and CNT: carbon nanotubes.

linear range (10–500 μM) with an ultralow detection limit of 7.95 μM and a quantification limit of 24.11 μM was obtained. Finally, real sample validation using serum samples (97%) and excellent recovery was observed. Meanwhile, reproducibility and stability studies confirmed the robustness of the platform. Collectively, a scalable, low sample volume, and low-cost route for the development of portable electrochemical biosensors was established, with strong potential for point-of-care testing (PoCT) of uric acid and broader applications in clinical diagnostics.

Conflicts of interest

There are no conflicts to declare.

Data availability

The data supporting this article have been included in the main article and/or as part of the supplementary information (SI).

Acknowledgements

The authors gratefully acknowledge the financial support from the BITS BioCyTiH Foundation (Grant No. BBF/BITS(H)/FY2022-23/BCPS-114). The authors also thank the BITS Pilani, Hyderabad Campus, for providing the research infrastructure and the Central Analytical Laboratory for the access to the characterization facilities. All experiments were performed in accordance with the Guidelines of the Medical Centre at BITS Pilani, Hyderabad Campus, and approved by the Medical Officer of the Medical Centre at BITS Pilani, Hyderabad Campus. Informed consents were obtained from the human participants of this study.

References

1 M. Kuwabara, T. Kodama, R. Ae, M. Kanbay, A. Andres-Hernando, C. Borghi, I. Hisatome and M. A. Lanaspa, Update in uric acid, hypertension, and cardiovascular diseases, *Hypertens. Res.*, 2023, **46**, 1714–1726, DOI: 10.1038/s41440-023-01273-3.

2 C. S. Kuo, C. M. Hwu, Y. H. Lin, Y. H. Huang, W. Y. Kao, M. J. Weih, L. C. Hsiao, C. F. Kwok and L. T. Ho, Portable electrochemical blood uric acid meter, *J. Clin. Lab. Anal.*, 2002, **16**, 109–114, DOI: 10.1002/jcla.10030.

3 J. C. Chen, H. H. Chung, C. T. Hsu, D. M. Tsai, A. S. Kumar and J. M. Zen, A disposable single-use electrochemical sensor for the detection of uric acid in human whole blood, *Sens. Actuators, B*, 2005, **110**, 364–369, DOI: 10.1016/j.snb.2005.02.026.

4 J. A. Muñoz, M. López-Mesas and M. Valiente, Development and validation of a simple determination of urine metabolites (oxalate, citrate, uric acid and creatinine) by capillary zone electrophoresis, *Talanta*, 2010, **81**, 392–397, DOI: 10.1016/j.talanta.2009.12.014.

5 Z. H. Sheng, X. Q. Zheng, J. Y. Xu, W. J. Bao, F. Bin Wang and X. H. Xia, Electrochemical sensor based on nitrogen doped graphene: Simultaneous determination of ascorbic acid, dopamine and uric acid, *Biosens. Bioelectron.*, 2012, **34**, 125–131, DOI: 10.1016/j.bios.2012.01.030.

6 X. Chen, G. Wu, Z. Cai, M. Oyama and X. Chen, Advances in enzyme-free electrochemical sensors for hydrogen peroxide, glucose, and uric acid, *Microchim. Acta*, 2014, **181**, 689–705, DOI: 10.1007/s00604-013-1098-0.

7 F. W. L. Silva, B. R. Freire, C. S. C. Lopes, F. D. Marques, B. S. Archanjo, E. S. Ribeiro, R. E. Santelli and F. H. Cincotto, Cylindrical 3D-printed electrode based on carbon

black and polylactic acid: an approach for electrochemical detection of the bithionol drug, *Ionics*, 2025, **31**, 6343–6352, DOI: 10.1007/s11581-025-06239-8.

8 P. M. Kalligosfyri, C. Miller, S. Cinti and B. A. Patel, 3D printed electrode-microwell system: a novel electrochemical platform for miRNA detection, *Microchim. Acta*, 2025, **192**, 330, DOI: 10.1007/s00604-025-07190-1.

9 L. S. Da Silva, L. R. G. Silva, H. S. Pittner, J. S. Stefano, D. Vanzin, R. M. Dornellas, B. C. Janegitz, L. V. de Faria, A. Galli, C. L. Handa and D. P. Rocha, Carbon black-integrated polylactic acid 3D-printed sensors for the voltammetric determination of pyrogallic acid: Experimental and computational insights, *Electrochim. Acta*, 2025, **541**, 147339, DOI: 10.1016/j.electacta.2025.147339.

10 H. H. Bin Hamzah, O. Keattch, D. Covill and B. A. Patel, The effects of printing orientation on the electrochemical behaviour of 3D printed acrylonitrile butadiene styrene (ABS)/carbon black electrodes, *Sci. Rep.*, 2018, **8**, 1–8, DOI: 10.1038/s41598-018-27188-5.

11 T. T. Conrado, E. R. Pedão, V. S. Ferreira, K. Motta, A. C. A. Silva, R. A. B. da Silva, J. M. Petroni and B. G. Lucca, Sensitive, Integrated, Mass-produced, Portable and Low-cost Electrochemical 3D-printed Sensing Set (SIMPLE-3D-SenS): A promising analytical tool for forensic applications, *Sens. Actuators, B*, 2025, **427**, 137215, DOI: 10.1016/j.snb.2024.137215.

12 K. Dalvand, A. Ghiasvand, S. Keshan-Balavandy, F. Li and M. Breadmore, A simple 3D printed microfluidic device for point-of-care analysis of urinary uric acid, *Aust. J. Chem.*, 2023, **76**, 74–80, DOI: 10.1071/CH22180.

13 V. Katic, P. L. Dos Santos, M. F. Dos Santos, B. M. Pires, H. C. Loureiro, A. P. Lima, J. C. M. Queiroz, R. Landers, R. A. A. Muñoz and J. A. Bonacin, 3D Printed Graphene Electrodes Modified with Prussian Blue: Emerging Electrochemical Sensing Platform for Peroxide Detection, *ACS Appl. Mater. Interfaces*, 2019, **11**, 35068–35078, DOI: 10.1021/acsami.9b09305.

14 Y. Kadri, I. Bekri-Abbess and P. Herrasti, Highly Sensitive Enzyme-free Sensor Based on a Carbon Paste Electrode Modified with Binary Zinc Oxide/Polyaniline Nanocomposites for Dopamine, Ascorbic Acid and Uric Acid Sensing, *Electroanalysis*, 2023, **35**, 1–14, DOI: 10.1002/elan.202200248.

15 N. Sittihakote, P. Danvirutai, S. Anutrakulchai, A. Tuantranont and C. Srichan, Empowering an Acute Kidney Injury 3D Graphene-Based Sensor Using Extreme Learning Machine, *ACS Omega*, 2024, **9**, 21276–21286, DOI: 10.1021/acsomega.4c01315.

16 C. L. Gonzalez-Gallardo, N. Arjona, L. Álvarez-Contreras and M. Guerra-Balcázar, Electrochemical creatinine detection for advanced point-of-care sensing devices: a review, *RSC Adv.*, 2022, **12**, 30785–30802, DOI: 10.1039/d2ra04479j.

17 D. L. Glasco, A. Sheelam, N. H. B. Ho and J. G. Bell, Smartphone-based detection of levodopa in human sweat using 3D printed sensors, *Anal. Chim. Acta*, 2023, **1273**, 341546, DOI: 10.1016/j.aca.2023.341546.

18 R. M. Cardoso, D. M. H. Mendonça, W. P. Silva, M. N. T. Silva, E. Nossol, R. A. B. da Silva, E. M. Richter and R. A. A. Muñoz, 3D printing for electroanalysis: From multiuse electrochemical cells to sensors, *Anal. Chim. Acta*, 2018, **1033**, 49–57, DOI: 10.1016/j.aca.2018.06.021.

19 A. Morais, D. P. Rocha, M. L. Felsner and A. Galli, Sustainable validated methodology for enzymeless determination of Tyrosine using 3D-printed PLA/CB electrodes in synthetic urine, *Talanta Open*, 2025, **11**, 100469, DOI: 10.1016/j.talo.2025.100469.

20 M. Parrilla, N. Claes, C. Toyos-Rodríguez, C. E. M. K. Dricot, A. Steijlen, S. Lebeer, S. Bals and K. De Wael, Wearable 3D-printed solid microneedle voltammetric sensors based on nanostructured gold for uric acid monitoring, *Biosens. Bioelectron.*, 2025, **289**, 117934, DOI: 10.1016/j.bios.2025.117934.

21 M. N. Islam and R. B. Channon, Electrochemical sensors, *Bioeng. Innovative Solutions Cancer*, 2019, 47–71, DOI: 10.1016/B978-0-12-813886-1.00004-8.

22 F. Gao, C. Liu, L. Zhang, T. Liu, Z. Wang, Z. Song, H. Cai, Z. Fang, J. Chen, J. Wang, M. Han, J. Wang, K. Lin, R. Wang, M. Li, Q. Mei, X. Ma, S. Liang, G. Gou and N. Xue, Wearable and flexible electrochemical sensors for sweat analysis: a review, *Microsyst. Nanoeng.*, 2023, **9**, 1–21, DOI: 10.1038/s41378-022-00443-6.

23 Y. G. Park, S. Lee and J. U. Park, Recent progress in wireless sensors for wearable electronics, *Sensors*, 2019, **19**, 1–34, DOI: 10.3390/s19204353.

24 Y. Liu, Y. Dong, M. Hui, L. Xu, L. Ye, J. Lv, L. Yang and Y. Cui, A biosensing array for multiplex clinical evaluation of glucose, creatinine, and uric acid, *Biosens. Bioelectron.*, 2023, **241**, 115699, DOI: 10.1016/j.bios.2023.115699.

25 S. R. S. Pour, D. Calabria, A. Emamiamin, E. Lazzarini, A. Pace, M. Guardigli, M. Zangheri and M. Mirasoli, Microfluidic-Based Non-Invasive Wearable Biosensors for Real-Time Monitoring of Sweat Biomarkers, *Biosensors*, 2024, **14**(1), 29, DOI: 10.3390/bios14010029.

26 A. Singh, A. Sharma, A. Ahmed, A. K. Sundramoorthy, H. Furukawa, S. Arya and A. Khosla, Recent advances in electrochemical biosensors: Applications, challenges, and future scope, *Biosensors*, 2021, **11**, 1–31, DOI: 10.3390/bios11090336.

27 R. Kale, M. K. Das, A. D. Gowda, S. A. Raut, J. Pannikkandathil, S. Bodake, R. M. Borkar, S. Pahal and S. Kumar, Direct Printing of an Electrochemical Device and Its Interface with Paper for Uric Acid Detection in Human Sweat, *ACS Appl. Bio Mater.*, 2025, **8**, 870–878, DOI: 10.1021/acsabm.4c01706.

28 S. Meng, Y. Liu, L. Wang, X. Ji, Y. Chen, T. Zheng, J. Yu and H. Feng, Graphene-Based Flexible Sensors for Simultaneous Detection of Ascorbic Acid, Dopamine, and Uric Acid, *Front. Bioeng. Biotechnol.*, 2021, **9**, 1–12, DOI: 10.3389/fbioe.2021.726071.

29 R. M. Cardoso, P. R. L. Silva, A. P. Lima, D. P. Rocha, T. C. Oliveira, T. M. do Prado, E. L. Fava, O. Fatibello-Filho, E. M. Richter and R. A. A. Muñoz, 3D-Printed graphene/polylactic acid electrode for bioanalysis: Biosensing of glucose and simultaneous determination of uric acid and nitrite in

biological fluids, *Sens. Actuators, B*, 2020, **307**, 127621, DOI: 10.1016/j.snb.2019.127621.

30 P. Dutta, V. Sharma, H. Bhardwaj, V. V. Agrawal and G. S. Rajesh, Fabrication of Electrochemical Biosensor Using Zinc Oxide Nanoflowers for the Detection of Uric Acid, *Mapan - J. Metrol. Soc. India*, 2022, **37**, 585–595, DOI: 10.1007/s12647-022-00598-7.

31 S. S. Chaus, S. Lal, A. SP and P. G. Bahubalindruni, A flexible and highly sensitive non-enzymatic electrochemical sensing platform with readout electronics for sensing uric acid in human urine: Towards devices, *Electrochim. Acta*, 2025, **539**, 147114, DOI: 10.1016/j.electacta.2025.147114.

32 W. Yang, J. Fei, W. Xu, H. Jiang, M. Sakran, J. Hong, W. Zhu and X. Zhou, A biosensor based on the biomimetic oxidase Fe3O4@MnO2 for colorimetric determination of uric acid, *Colloids Surf., B*, 2022, **212**, 112347, DOI: 10.1016/j.colsurfb.2022.112347.

33 K. Fan, J. Zeng, C. Yang, G. Wang, K. Lian, X. Zhou, Y. Deng and G. Liu, Digital Quantification Method for Sensitive Point-of-Care Detection of Salivary Uric Acid Using Smartphone-Assisted μpADs, *ACS Sens.*, 2022, **7**, 2049–2057, DOI: 10.1021/acssensors.2c00854.

34 S. Y. Lee, D. S. Ciou, H. Y. Lee, J. Y. Chen, Y. C. Wei and M. D. Shieh, Portable Electrochemical System and Platform with Point-of-Care Determination of Urine Albumin-to-Creatinine Ratio to Evaluate Chronic Kidney Disease and Cardiorenal Syndrome, *Biosensors*, 2024, **14**(10), 463, DOI: 10.3390/bios14100463.

35 D. Desai, A. Kumar, D. Bose and M. Datta, Ultrasensitive sensor for detection of early stage chronic kidney disease in human, *Biosens. Bioelectron.*, 2018, **105**, 90–94, DOI: 10.1016/j.bios.2018.01.031.

36 S. Fabre, P. Clerson, J. M. Launay, J. F. Gautier, T. Vidal-Trecan, J. P. Riveline, A. Platt, A. Abrahamsson, J. N. Miner, G. Hughes, P. Richette and T. Bardin, Accuracy of the HumaSens plus point-of-care uric acid meter using capillary blood obtained by fingertip puncture, *Arthritis Res. Ther.*, 2018, **20**, 1–9, DOI: 10.1186/s13075-018-1585-0.

37 V. N. Ataide, D. P. Rocha, A. de Siervo, T. R. L. C. Paixão, R. A. A. Muñoz and L. Angnes, Additively manufactured carbon/black-integrated polylactic acid 3Dprintedsensor for simultaneous quantification of uric acid and zinc in sweat, *Microchim. Acta*, 2021, **188**, 1–11, DOI: 10.1007/s00604-021-05007-5.

38 M. J. C. Matter, M. Rjeb, A. Labzour, A. Rjeb, S. Sayouri, M. C. El Idrissi, S. Massey, A. Adnot, D. Roy and C. M. Society, Contribution to the study by X-Ray photoelectron spectroscopy of the natural aging of the 2, *Exp. Proc.*, 2004, **5**, 1–5.

39 M. Parrilla, N. Claes, C. Toyos-Rodríguez, C. E. M. K. Dricot, A. Steijlen, S. Lebeer, S. Bals and K. De Wael, Wearable 3D-printed solid microneedle voltammetric sensors based on nanostructured gold for uric acid monitoring, *Biosens. Bioelectron.*, 2025, **289**, 117934, DOI: 10.1016/j.bios.2025.117934.

40 E. Gaya, N. Menendez, E. Mazario and P. Herrasti, Fe3O4-Nanoparticle-Modified Sensor for the Detection of Dopamine, Uric Acid and Ascorbic Acid, *Chem*, 2023, **11**(2), 79, DOI: 10.3390/chemosensors11020079.

41 A. O. Alves, L. V. de Faria, N. M. Caldas, A. G. Batista, S. F. L. do Nascimento, B. E. Danho, D. A. Peixoto, E. Nossol, D. P. Rocha, F. S. Semaan, W. F. Pacheco and R. M. Dornellas, 3D-printed carbon black/polylactic acid electrode modified with silver particles: a powerful alternative and cost-effective sensor for nitrate sensing in real water samples, *J. Solid State Electrochem.*, 2025, **29**, 1217–1225, DOI: 10.1007/s10008-024-05919-1.

42 S. Kumar, J. M. Mohan, K. Amreen, S. K. Dubey and S. Goel, A miniaturized unmodified toray paper-based electrochemical sensing platform for antipsychotic drug analysis, *Sens. Actuators, A*, 2023, **360**, 114520, DOI: 10.1016/j.sna.2023.114520.

43 S. Kumar, A. K. Bhagat, M. Bhaiyya, K. Amreen, S. K. Dubey and S. Goel, A Machine Learning Approach for Simultaneous Electrochemical Detection of Dopamine and Serotonin in an Optimized Carbon Thread-Based Miniaturized Device, *IEEE Sens. J.*, 2024, **24**, 21378–21385, DOI: 10.1109/JSEN.2024.3386655.

44 J. M. Mohan, S. Kumar, K. Amreen, A. Javed, S. K. Dubey and S. Goel, Disposable paper-based miniaturized device for sensing of phthalates, *IEEE Sens. J.*, 2023, **23**(14), 16189–16196, DOI: 10.1109/JSEN.2023.3277797.

45 Z. Xu, M. q. Zhang, H. q. Zou, J. s. Liu, D. z. Wang, J. Wang and L. d. Wang, Non-enzymatic electrochemical detection of uric acid with electrodeposited Nafion film, *J. Electroanal. Chem.*, 2019, **841**, 129–134, DOI: 10.1016/j.jelechem.2019.04.028.

46 A. G. Cardoso, H. Viltres, G. A. Ortega, V. Phung, R. Grewal, H. Mozaffari, S. R. Ahmed, A. R. Rajabzadeh and S. Srinivasan, Electrochemical sensing of analytes in saliva: Challenges, progress, and perspectives, *TrAC, Trends Anal. Chem.*, 2023, **160**, 116965, DOI: 10.1016/j.trac.2023.116965.

47 M. Yang, H. Wang, P. Liu and J. Cheng, A 3D electrochemical biosensor based on Super-Aligned Carbon NanoTube array for point-of-care uric acid monitoring, *Biosens. Bioelectron.*, 2021, **179**, 113082, DOI: 10.1016/j.bios.2021.113082.

48 P. Noppawan, J. Jakmunee, A. J. Hunt, N. Supanchaiyamat, S. Sangon, J. Lerdsri, T. Kruatian and J. Upan, Sustainable uric acid sensor based on a lab-fabricated electrode modified with rice straw-derived carbon materials, *Sci. Rep.*, 2025, **15**, 18380, DOI: 10.1038/s41598-025-03405-w.

49 W. Liu, Y. Nie, M. Zhang, K. Yan, M. Wang, Y. Guo and Q. Ma, A novel nanosponge–hydrogel system-based electrochemiluminescence biosensor for uric acid detection, *Luminescence*, 2022, **37**, 1524–1531, DOI: 10.1002/bio.4326.

50 S. Verma, J. Choudhary, K. P. Singh, P. Chandra and S. P. Singh, Uricase grafted nanoconducting matrix based electrochemical biosensor for ultrafast uric acid detection in human serum samples, *Int. J. Biol. Macromol.*, 2019, **130**, 333–341, DOI: 10.1016/j.ijbiomac.2019.02.121.